Supplementary Information for:

Structure of the agonist-bound neurotensin receptor

Jim F. White, Nicholas Noinaj, Yoko Shibata, James Love, Brian Kloss, Feng Xu, Jelena Gvozdenovic-Jeremic, Priyanka Shah, Joseph Shiloach, Christopher G. Tate, Reinhard Grisshammer

Supplementary Discussion

Pharmacological characterization of NTS1-GW5

Ligand binding experiments (Fig. S3, Table S2) showed that the affinity of NTS1-GW5 for the agonist NT was similar to that of the wild-type receptor, but the apparent IC_{50} value for the neutral antagonist SR48692 (ref.[1]) was 130-200 fold higher than the corresponding wild-type value. The shift in IC_{50} values may be caused partly by a change in affinity of SR48692 to NTS1-GW5, and/or because SR48692 and [^{3}H]NT binding to NTS1-GW5 did not achieve equilibrium under the experimental conditions because of the significant change in the off-rate of [^{3}H]NT for this mutant.

In addition, NTS1-GW5 showed reduced sensitivity of agonist binding in the presence of Na^+ ions as observed for the thermostabilized NTS1 mutant NTS1-7m (ref.[2]) possibly indicating a high-affinity agonist conformation of NTS1-GW5. In contrast to wild-type NTS1, the presence of NaCl does not increase the dissociation of [^{3}H]NT (Fig. S3), and the IC_{50} value for NaCl is 5-fold higher compared to wild-type NTS1 (Fig. S3, Table S2). A recent high-resolution structure of the antagonist-bound adenosine A_{2a} receptor identified a putative Na^+ ion bound to the highly conserved $D^{2.50}$ acting as a negative allosteric effector on agonist binding[3]. As suggested for the A_{2a} receptor, the binding pocket for the Na^+ ion collapses in the active state, with high-affinity agonist binding and the presence of Na^+ ions being mutually exclusive. The reduced sensitivity of NTS1-GW5 towards Na^+ ions may indicate a high-affinity conformation preventing Na^+ ions from entering the receptor core. Of interest, mutation of $D113^{2.50}$ in NTS1 into an alanine residue abolishes the Na^+ ion effect[4] linking this conserved residue to the Na^+ ion dependent modulation of agonist affinity.

In G protein coupling assays NTS1-GW5 did not catalyze nucleotide exchange at Gαq in response to NT (Fig. S3), suggesting that the stabilizing mutations may have limited the ability to propagate the agonist-induced conformational change at the ligand binding pocket to the re-arrangement of the intracellular face of the receptor required for G protein binding and activation. The pharmacological profile of NTS1-GW5 is similar to that of $A_{2A}R$ thermostabilized in an agonist-bound state, which showed unchanged affinity for agonists, decreased affinity for antagonists and minimal ability to activate G proteins[5].

The NT_{8-13} binding site

NTS1 has been subjected to extensive site-directed mutagenesis studies to define ligand-receptor interactions, predominantly by mutating aromatic and charged amino acid residues[6-9]. These results are fully consistent with the structure of NT_{8-13}-bound NTS1. The R8 side chain of NT_{8-13} forms extensive van der Waals interactions with $F344^{7.28}$ and the mutant F344A reduced agonist binding by 5-10 fold[6,9]. The phenyl side chain of $F331^{6.58}$ intercalates between the NT_{8-13} sides chains R9 and L13 and the mutant F331A lowered NT binding by 10-fold[8]. The P10 side chain in NT_{8-13} forms extensive van der Waals interactions with $W339^{ECL3}$ and the mutant W339A showed reduced agonist affinity of 10-fold[6,9]. Y11 in NT_{8-13} is important for receptor binding as it forms a hydrogen bond with the backbone carbonyl of L55 (N terminal region) and van der Waals interactions with $H132^{ECL1}$ and $H133^{ECL1}$, and $V224^{ECL2}$; the NT mutant Y11A bound to NTS1 with a 6000-fold lower affinity[10]. Deletion of residues 45-60 from NTS1 resulted in 3000-fold lower NT binding[11] reflecting the loss of a stabilizing hydrogen bond by removal of L55, but these data also probably emphasize the structural role of the proximal end of the N-terminus capping the agonist binding site. The backbone carbonyl of I12 in NT_{8-13} forms a hydrogen bond to the hydroxyl of $Y347^{7.31}$; the NTS1 mutants Y347F and Y347A showed weak binding or no binding of NT, respectively[6,8]. The L13 side chain of NT makes van der Waals interactions with $M208^{ECL2}$ and the NTS1 mutant M208A showed a 10-fold reduction in agonist

affinity[8]. In the crystal structure, the carboxylate group at the C-terminus of NT_{8-13} is predicted to make a salt bridge with the NH1 and NH2 atoms of $R327^{6.54}$ and a hydrogen bond with the hydroxyl group of $Y146^{3.29}$. Amidation of the C-terminus of NT resulted in a 500-fold reduction in affinity compared to NT_{8-13} (ref.[10]).

Abbreviations

DM, n-decyl-β-D-maltopyranoside
ECL, extracellular loop
ICL, intracellular loop
LMNG, lauryl maltose neopentyl glycol (2,2-didecylpropane-1,3-bis-β-D-maltopyranoside)
T4L, cysteine-free bacteriophage T4 lysozyme (C54T, C97A)
TM, transmembrane domain

Acknowledgements

The production of NTS1 in insect cells was done at the Protein Expression Laboratory, Advanced Technology Program, SAIC-Frederick, National Cancer Institute, Frederick, MD, USA. DNA sequence analysis was performed by the National Institute of Neurological Disorders and Stroke DNA Sequencing Facility. Peptides were synthesized at the Center for Biologics Evaluation and Research (Food and Drug Administration, Bethesda, MD, USA). We thank Brian Kobilka, Andrew Kruse and Aashish Manglik (Stanford University, USA) for insight into crystallization approaches; Irina Kufareva (UC San Diego, USA) for discussion about T4L insertion strategies; and Vadim Cherezov, Wei Liu, Fei Xu, and Ray Stevens (The Scripps Research Institute, La Jolla, USA) for an initial HT-LCP-FRAP and LCP-Tm experiment. We thank Stefano Costanzi (American University, Washington DC, USA) for Supplementary Figure S1 and Marc Baldus (Utrecht University, The Netherlands) for the NMR pdb file. We thank Danny Axford at beamline I24 (Diamond Light Source, Harwell), and Tony Warne and Pat Edwards (MRC-LMB) who screened initial crystals for quality at I24.

Table S1: Denaturation temperatures (T_m) of NTS1-GW5-T4L and wild-type NTS1 in detergent solution.

Denaturation profiles were recorded in the presence of [^{3}H]NT. All values are given ± SE from 3-4 independent experiments conducted as single data points.

	Apparent T_m (ºC)	Detergent	ΔT_m (ºC)
Wild-type NTS1	26.0 ± 0.8	DM	
NTS1-GW5-T4L	49.9 ± 0.7	DM	23.9
Wild-type NTS1	39.8 ± 0.5	LMNG	
NTS1-GW5-T4L	58.7 ± 0.1	LMNG	18.9

Table S2: Pharmacological properties of NTS1-GW5-T4L.

All binding experiments were conducted with NTS1 constructs in urea-washed P2 insect cell membranes. NTS1-GW5-T4L with T4L replacing most of ICL3 was compared to NTS1-GW5 containing ICL3. Wild-type NTS1 was included as a reference. All values are given ± SE from 3 independent experiments conducted as single data points. K_d, equilibrium dissociation constant (saturation binding) but see note below; $IC_{50\ (SR48692)}$, half maximal inhibitory concentration of SR48692 on [^{3}H]NT binding; $IC_{50\ (NaCl)}$, half maximal inhibitory concentration of Na^+ ions on [^{3}H]NT binding. Ligand depletion was below 8% for saturation binding experiments, below 11% for competition experiments and below 6% for NaCl titration experiments. Note that all binding experiments using NTS1-GW5-T4L and NTS1-GW5 never reached equilibrium within the incubation time because of the very slow [^{3}H]NT off-rates. *, value for apparent dissociation constant.

	NTS1-GW5-T4L	**NTS1-GW5**	**Wild-type NTS1**
K_d (nM)	2.9 ± 0.1 *	2.5 ± 0.2 *	1.5 ± 0.1
$IC_{50\ (SR48692)}$ (nM)	1806 ± 289	1247 ± 253	9.3 ± 1.3
$IC_{50\ (NaCl)}$ (mM)	205 ± 51	184 ± 43	43 ± 10

Table S3: Data collection and refinement statistics.

Data Collection	**NTS1-GW5-T4L**
Number of crystals	1
λ (Å)	1.0
Space group	$P2_1$
Mol/ASU	1
Cell dimensions	
a, b, c (Å)	46.96, 69.62, 97.53
α, β, γ (º)	90, 101.7, 90
Resolution (Å)	30-2.80 (2.90-2.80)
Completeness (%)*	93.1 (86.4)
Redundancy*	2.4 (2.1)
R_{sym}†*	0.15 (0.65)
I / σ (I)*	5.6 (1.3)
Refinement	
Resolution (Å)	15-2.80
No. reflections	14956
R§/R_{free}¶	0.23/0.28
r.m.s. deviations	
Bonds (Å)	0.005
Angles (º)	1.014
Protein atoms	3435
Ligand atoms	88
Waters	23
B-factors (Å^2)	
NTS1-GW5-T4L	88.2
NTS1-GW5	85.6
T4L	92.3
NT_{8-13} peptide	93.4
Waters	65.9
Ramachandran Analysis¥	
Favored regions (%)	92.0
Allowed regions (%)	8.0
Outliers (%)	0.0

† Rsym = $\Sigma_{hkl,j}$ ($|I_{hkl}-\langle I_{hkl}\rangle|$) / $\Sigma_{hkl,j}$ I_{hkl}, where $\langle I_{hkl}\rangle$ is the average intensity for a set of j symmetry related reflections and I_{hkl} is the value of the intensity for a single reflection within a set of symmetry-related reflections.

§ R factor = Σ_{hkl} ($||F_o| - |F_c||$) / $\Sigma_{hkl}|F_o|$ where F_o is the observed structure factor amplitude and F_c is the calculated structure factor amplitude.

¶ R_{free} = $\Sigma_{hkl,T}$ ($||F_o| - |F_c||$) / $\Sigma_{hkl,T}|F_o|$, where a test set, T (5% of the data), is omitted from the refinement.

[¥] Performed using MolProbity[12].
[*] Indicates statistics for last resolution shell shown in parenthesis.

Table S4: Hydrogen bonds and salt bridges between NT_{8-13} and NTS1-GW5-T4L.

The analysis was performed using the PDBePISA server[13]. Abbreviations and symbols used are as follows: H, hydrogen bond; S, salt bridge; TM, transmembrane helix; N, amino-terminus; ECL, extracellular loop; *, modeled carboxyl group.

NT_{8-13} atoms		Distance (Å)	NTS1 atoms		Location in NTS1
Arg8	[NH1]	3.7 (H)	Asp56	[O]	N
Arg9	[NH1]	2.5 (H)	Phe331	[O]	TM6
Tyr11	[OH]	2.5 (H)	Leu55	[O]	N
Tyr11	[O]	2.8 (H)	Thr226	[OG1]	ECL2-β2
Ile12	[O]	3.1 (H)	Tyr347	[OH]	TM7
Leu13	[N]	3.6 (H)	Tyr146	[OH]	TM3
Leu13	[O]*	3.0 (S)	Arg327	[NH1]	TM6
Leu13	[O]*	2.4 (H,S)	Arg327	[NH2]	TM6
Leu13	[OXT]*	2.6 (H)	Tyr146	[OH]	TM3

Table S5: Potential intermolecular interactions of NTS1-GW5-T4L residues and NT_{8-13}.

The analysis was performed using the PDBePISA server. Abbreviations used are as follows: TM, transmembrane helix; N, amino-terminus; ECL, extracellular loop.

	NTS1 atoms	Location in NTS1
Asp54	[O] [C]	N
Leu55	[O] [CA] [CB] [CG] [CD2]	N
Asp56	[O] [N]	N
Val57	[CG2]	N
Asn127	[O]	TM2
Phe128	[CA] [O] [CB] [CG] [CD1] [CE1] [CE2] [CZ]	TM2
His132	[O] [CA] [CB] [CD2]	ECL1
His133	[CB]	ECL1
Tyr146	[CE2] [OH]	TM3
Arg149	[NH1]	TM3
Met204	[SD] [CE]	TM4
Met208	[SD] [CE]	ECL2-β1
Arg213	[CD] [NH1] [NH2]	ECL2
Val224	[CB] [CG1] [CG2]	ECL2-β2
Cys225	[O]	ECL2-β2
Thr226	[CA] [CB] [OG1]	ECL2-β2
Pro227	[CG] [CD]	ECL2-β2
Thr231	[CB] [OG1] [CG2]	ECL2
Val234	[CG1]	TM5
Ile238	[CG2]	TM5
Arg327	[NH1] [NH2]	TM6
Arg328	[CA] [O] [CB] [CD] [NE] [CZ] [NH1]	TM6
Phe331	[CA] [O] [CB] [CG] [CD1] [CD2] [CE1] [CE2] [CZ]	TM6
Cys332	[CA] [CB]	TM6
Ser335	[CA] [CB]	ECL3
Asp336	[OD1]	ECL3
Glu337	[CD] [OE1] [OE2]	ECL3
Trp339	[O] [C] [CB] [CG] [CD1] [CD2] [NE1] [CE2] [CE3] [CZ2] [CZ3] [CH2]	ECL3
Thr340	[O] [C]	ECL3
Thr341	[CA] [OG1] [CG2]	TM7
Phe344	[CA] [CB] [CG] [CD1] [CD2] [CE1] [CE2] [CZ]	TM7
Tyr347	[CB] [CG] [CD2] [CE1] [CE2] [CZ] [OH]	TM7
His348	[CD2] [CE1] [NE2]	TM7
Tyr351	[CD1] [CD2] [CE1] [CE2] [CZ] [OH]	TM7

Fig. S1: Phylogenetic dendrogram of class A GPCRs based on aligned sequences.

Receptors with solved crystal structures are highlighted. The classification by Fredriksson[14] of class A GPCRs into α-, β-, γ- and δ-groups is indicated by brackets.

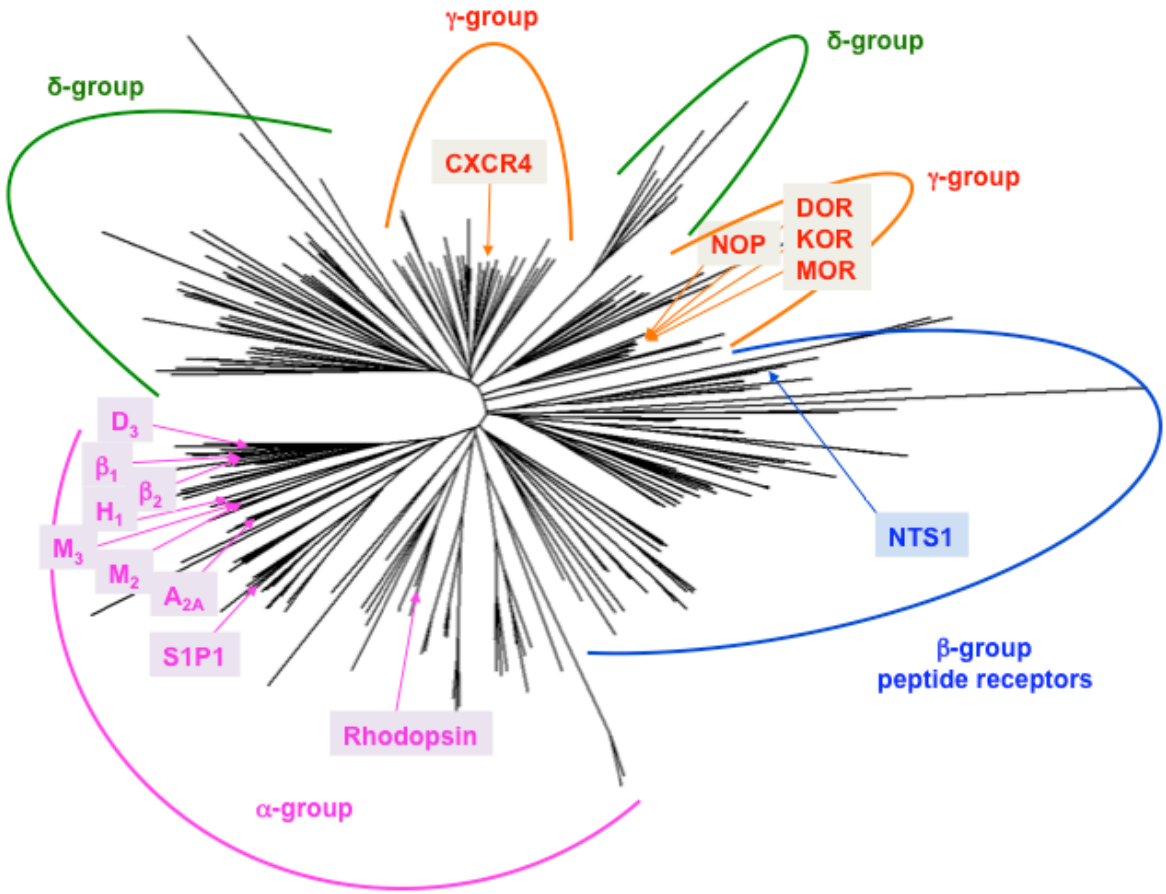

Fig. S2: Denaturation profiles of NTS1-GW5-T4L and wild-type NTS1 in detergent solution.

NTS1 was solubilized with detergent and heated at elevated temperatures for 30 min in the presence of [^{3}H]NT. Representative experiments conducted as single data points are shown. DM solubilized receptors: closed symbols; LMNG solubilized receptors: open symbols; NTS1-GW5-T4L in green, wild-type NTS1 in orange.

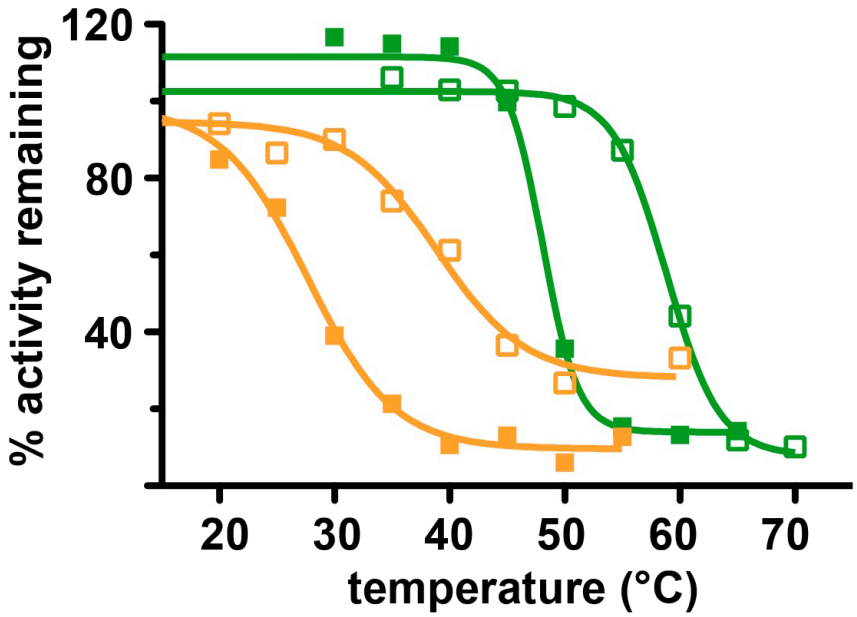

Fig. S3: Pharmacological properties of NTS1-GW5-T4L.

All binding experiments were conducted with NTS1 constructs in urea-washed P2 insect cell membranes. All panels have an identical color code: NTS1-GW5-T4L (green), NTS1-GW5 (purple), wild-type NTS1 (orange). In NTS1-GW5-T4L most of ICL3 is replaced with T4L, but NTS1-GW5 contains an ICL3 identical to that in NTS1. (a-c) [^{3}H]NT saturation binding; inset: Scatchard transformation. (d) Competition of agonist binding by the non-peptide antagonist SR48692. (e) Influence of Na^+ ions on agonist binding. (f) Agonist association and dissociation: [^{3}H]NT association (closed squares) was probed in TEBB buffer. Dissociation of agonist from NTS1 was determined by quantifying the amount of [^{3}H]NT remaining bound to receptors upon addition (arrow) of excess unlabeled NT in the presence (open circles) or absence of NaCl (closed circles). Representative experiments conducted in singles are shown for (a-f). (g) Agonist-stimulated activation of Gq protein: GDP/[^{35}S]GTPγS exchange assays contained purified Gαq, Gβ$_1$γ$_1$, [^{35}S]GTPγS and insect cell membranes with NTS1. Receptors were incubated with either no additional ligands (open bars), with NT (closed bars) or with the antagonist SR48692 (striped bars). Two experiments performed in duplicate gave similar results. Less than 4% of [^{35}S]GTPγS was consumed in the respective reactions.

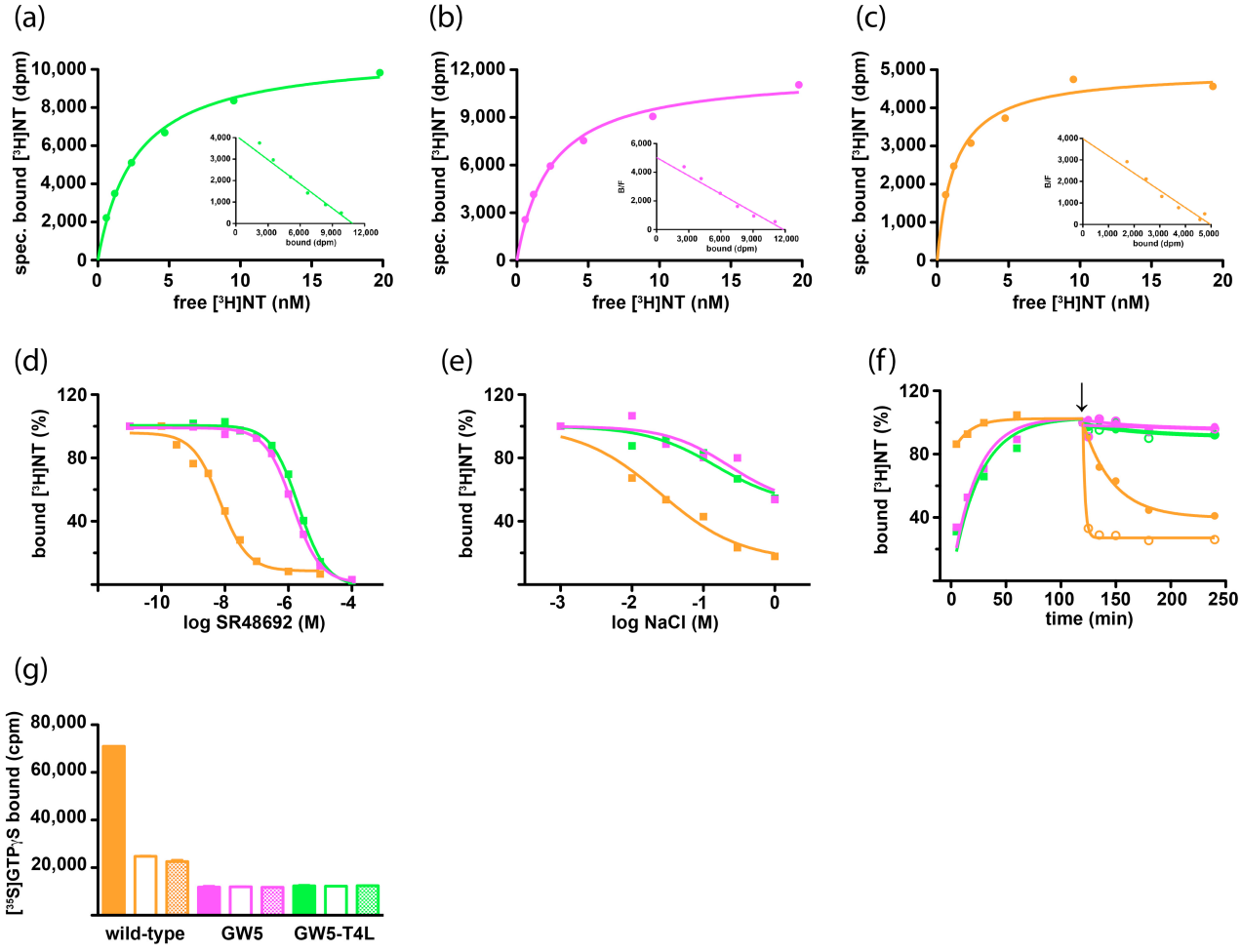

Fig. S4: Lattice packing of the NTS1-GW5-T4L crystal.

The receptor is depicted in green and T4L in pale brown. The NTS1-GW5-T4L molecules are arranged as rows of anti-parallel (a) and parallel dimers (b). The main crystal contacts are mediated through T4L. Minor contacts occur between T4L and ECL2 (d) and between T4L and ICL2 (not shown).

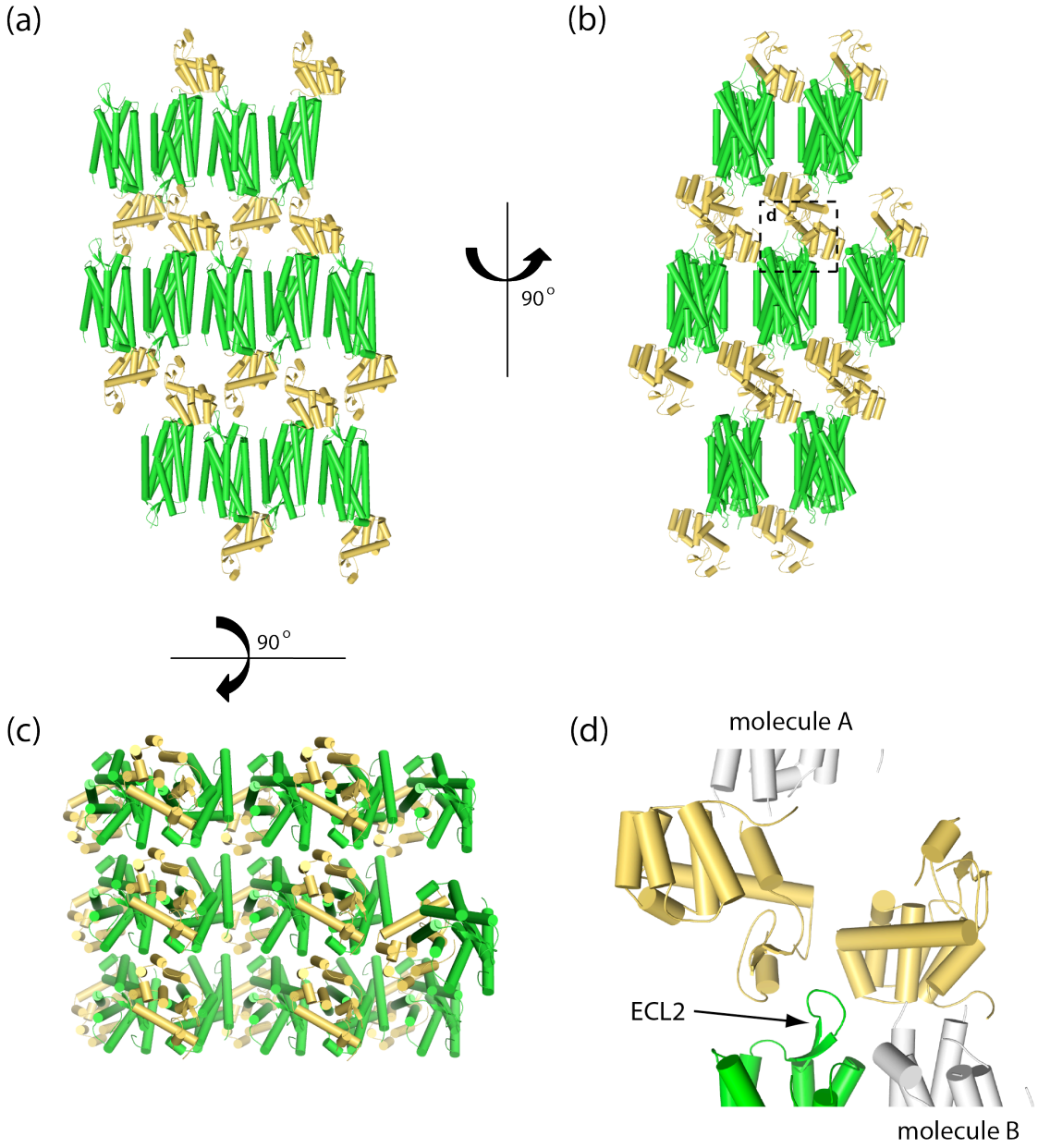

Fig. S5: Stereo view of the electron density of NTS1-GW5-T4L.

The quality of the electron density is depicted for TM6 as an example showing the $2F_o$-F_c map contoured at 1σ. Backbone residues of TM6 are in cartoon representation and amino acid side chains are shown as sticks.

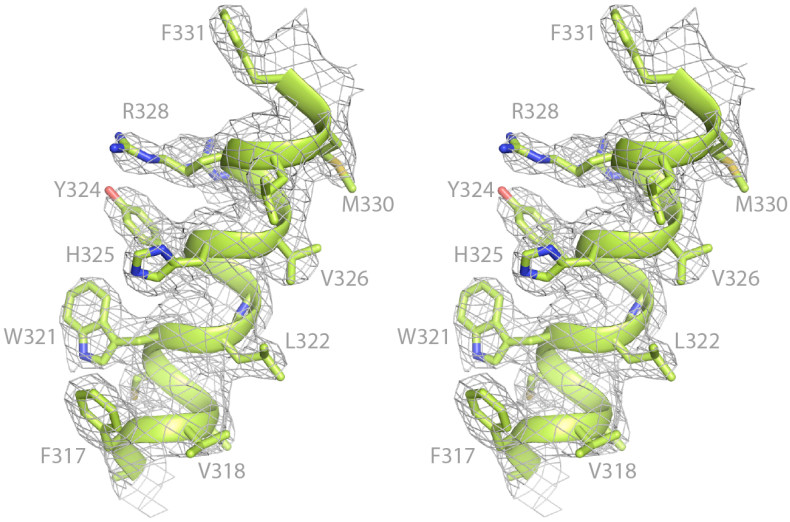

Fig. S6: Schematic representation of the rat NTS1-GW5-T4L.

The residues in white circles indicate regions that are well ordered in the crystal structure whereas the sequences in grey circles were not resolved in the structure. Stabilizing mutations are in purple circles (A86L$^{1.54}$, E166A$^{3.49}$, G215A, L310A$^{6.37}$, F358A$^{7.42}$, V360A$^{7.44}$; Ballesteros-Weinstein numbering[15] is in superscript). Helices (grey boxes) were defined using the Kabsch and Sander algorithm[16]. A yellow line indicates the disulphide bond between residues C142 and C225. Pink arrows denote the β-hairpin. The T4 lysozyme (yellow box) replaced intracellular loop 3 residues H269-R299.

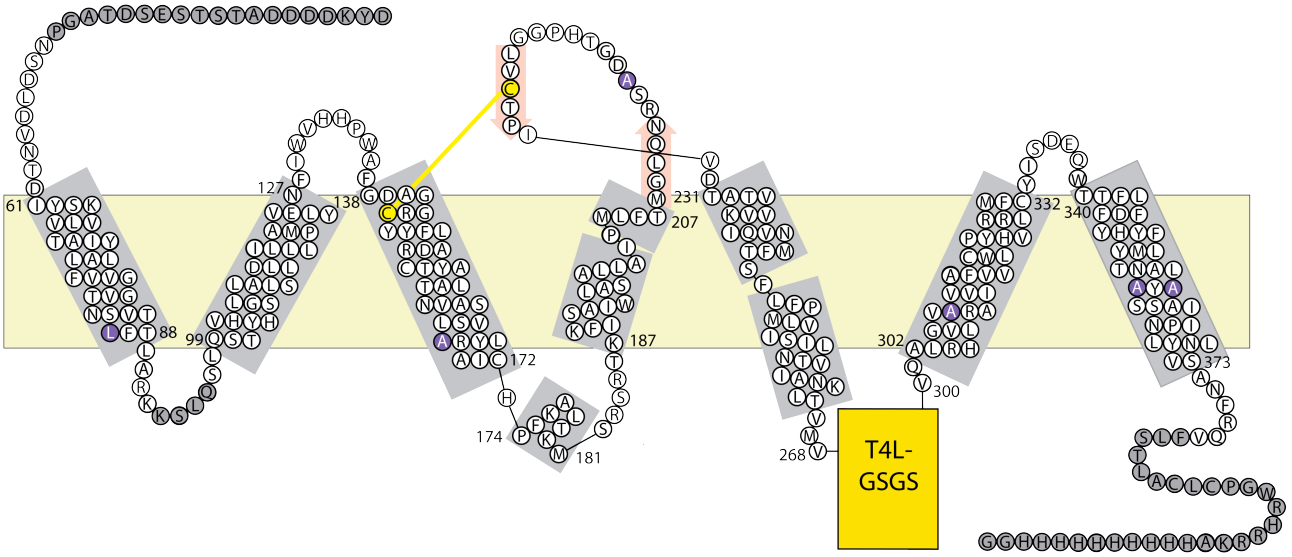

Fig. S7: Potential clash of G protein with NTS1-GW5.

The extended intracellular end of TM7 of NTS1-GW5 (green) covers space that is occupied by the C-terminal α-helix of Gαs (blue) in the β_2-adrenergic receptor - Gs protein complex[17] (PDB code 3SN6) or by the GαCT peptide (purple) in the active rhodopsin structure[18] (PDB code 3PQR). The transmembrane helices of rhodopsin and the β_2-adrenergic receptor were removed for clarity after alignment (PyMOL). The hydrogen bonds between N375 and Q378 of TM7 and A302 at the intracellular end of TM6 are indicated as dashed lines. This scenario assumes that the interaction of NTS1 with the C-terminal α-helix of Gαq is similar to that observed for the β_2-adrenergic receptor with Gαs and for rhodopsin with the GαCT peptide.

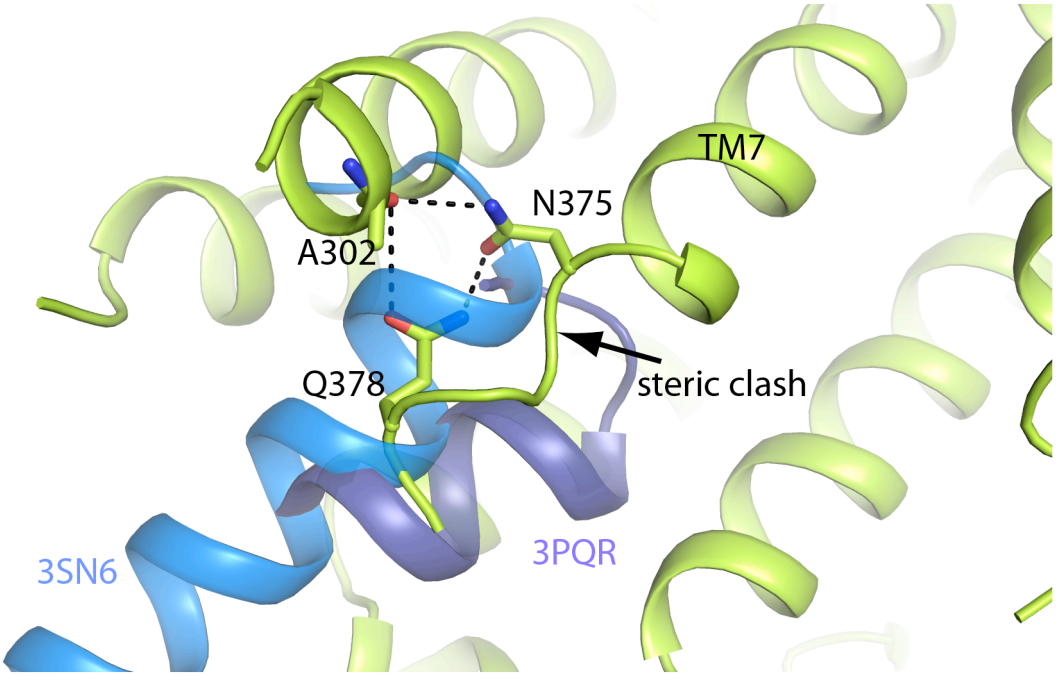

Fig. S8: Sequence differences between the rat and human NTS1.

The human wild-type NTS1 sequence[19] is 84% identical to the rat wild-type NTS1 sequence[20]. The differences were mapped onto the NTS1-GW5-T4L crystal structure and are indicated in blue. (a) Ribbon representation of NTS1. (b) Space filling model. (c) Sequence alignment between human and rat wild-type NTS1. The TM helices based on the NTS1-GW5-T4L structure are highlighted alternating in yellow and in green. The positions of the thermostabilizing mutations are indicated in bold blue letters. Vertical bars indicate identical amino acid residues in the rat and human wild-type NTS1 sequences.

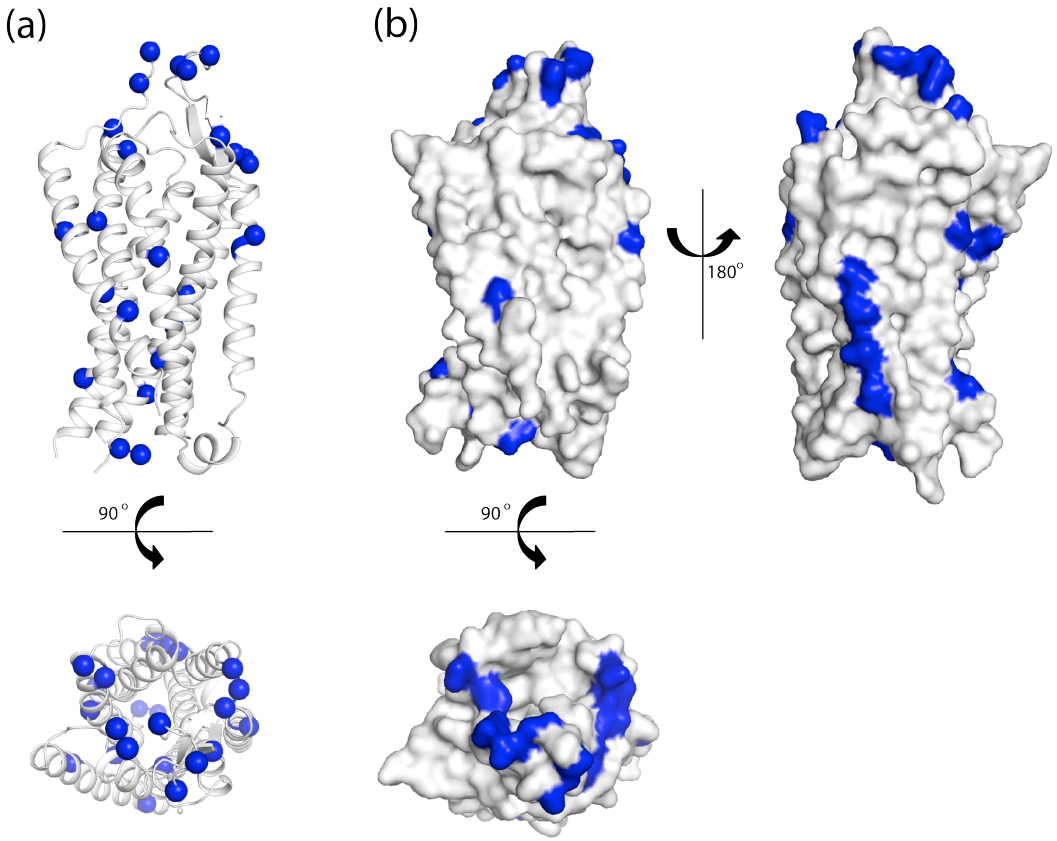

(c)

```
rat       1 MHLNSSVPQGTPGEPDAQPFSGPQSEMEATFLALSLSNGSGNTSESDTAG  50
            | |||| | |||| | | ||   |   |   ||    | ||| ||   |
human     1 MRLNSSAP-GTPGTPAADPFQRAQAGLEEALLAPGFGNASGNASERVLAA  49
                      TM1                          TM1       TM2
rat      51 PNSDLDVNTDIYSKVLVTAIYLALFVVGTVGNSVTAFTLARKKSLQSLQS 100
            | | ||||||||||||||| |||||||||||| |||||||||||||||||
human    50 PSSELDVNTDIYSKVLVTAVYLALFVVGTVGNTVTAFTLARKKSLQSLQS  99
                                    TM2          TM3
rat     101 TVHYHLGSLALSDLLILLLAMPVELYNFIWVHHPWAFGDAGCRGYYFLRD 150
            |||||||||||||||| ||||||||||||||||||||||||||||||||||
human   100 TVHYHLGSLALSDLLTLLLAMPVELYNFIWVHHPWAFGDAGCRGYYFLRD 149
```

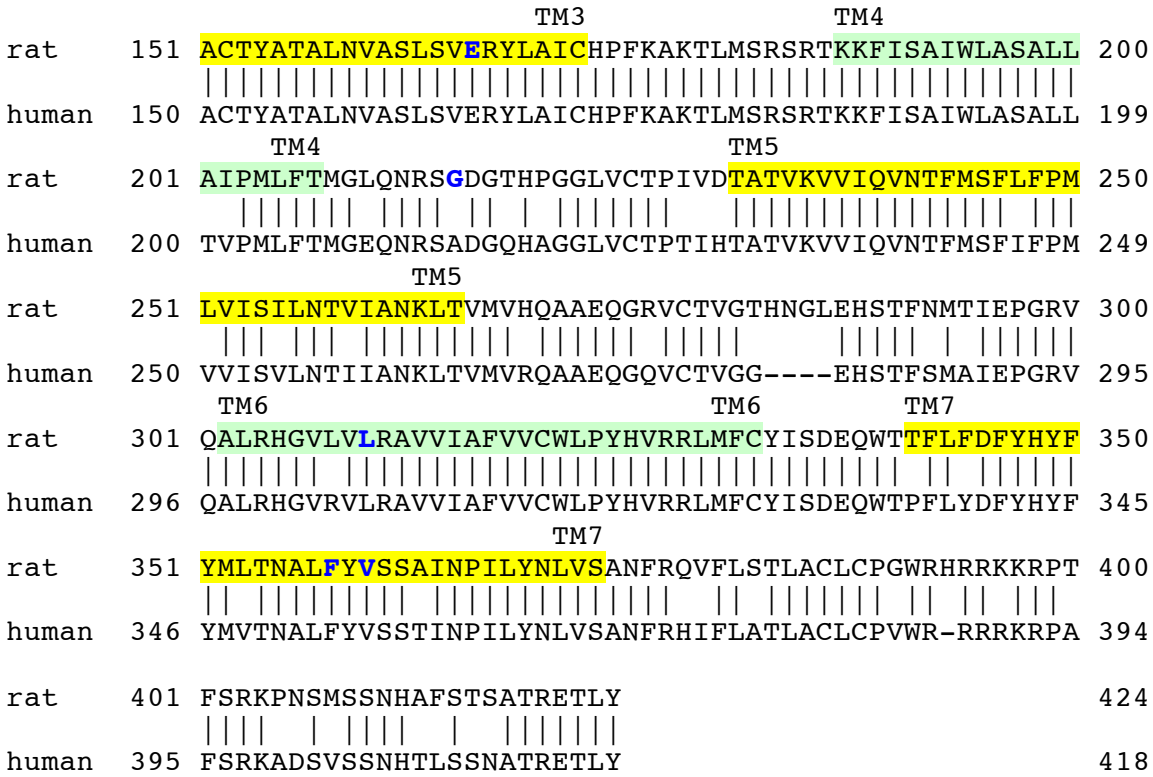
TM3
TM4
rat 151 ACTYATALNVASLSVERYLAICHPFKAKTLMSRSRTKKFISAIWLASALL 200
human 150 ACTYATALNVASLSVERYLAICHPFKAKTLMSRSRTKKFISAIWLASALL 199
TM4
TM5
rat 201 AIPMLFTMGLQNRSGDGTHPGGLVCTPIVDTATVKVVIQVNTFMSFLFPM 250
human 200 TVPMLFTMGEQNRSADGQHAGGLVCTPTIHTATVKVVIQVNTFMSFIFPM 249
TM5
rat 251 LVISILNTVIANKLTVMVHQAAEQGRVCTVGTHNGLEHSTFNMTIEPGRV 300
human 250 VVISVLNTIIANKLTVMVRQAAEQGQVCTVGG----EHSTFSMAIEPGRV 295
TM6
TM6
TM7
rat 301 QALRHGVLVLRAVVIAFVVCWLPYHVRRLMFCYISDEQWTTFLFDFYHYF 350
human 296 QALRHGVRVLRAVVIAFVVCWLPYHVRRLMFCYISDEQWTPFLYDFYHYF 345
TM7
rat 351 YMLTNALFYVSSAINPILYNLVSANFRQVFLSTLACLCPGWRHRRKKRPT 400
human 346 YMVTNALFYVSSTINPILYNLVSANFRHIFLATLACLCPVWR-RRRKRPA 394
rat 401 FSRKPNSMSSNHAFSTSATRETLY 424
human 395 FSRKADSVSSNHTLSSNATRETLY 418

Fig. S9: Schematic drawing of the NT_{8-13} binding pocket.

This drawing was modified from the output of LIGPLOT[21]. NT_{8-13} residues are labeled in blue. Receptor residues are shown in green and black (hydrophobic residues). Potential hydrogen bonds (<3.2Å) are indicated as green dashed lines.

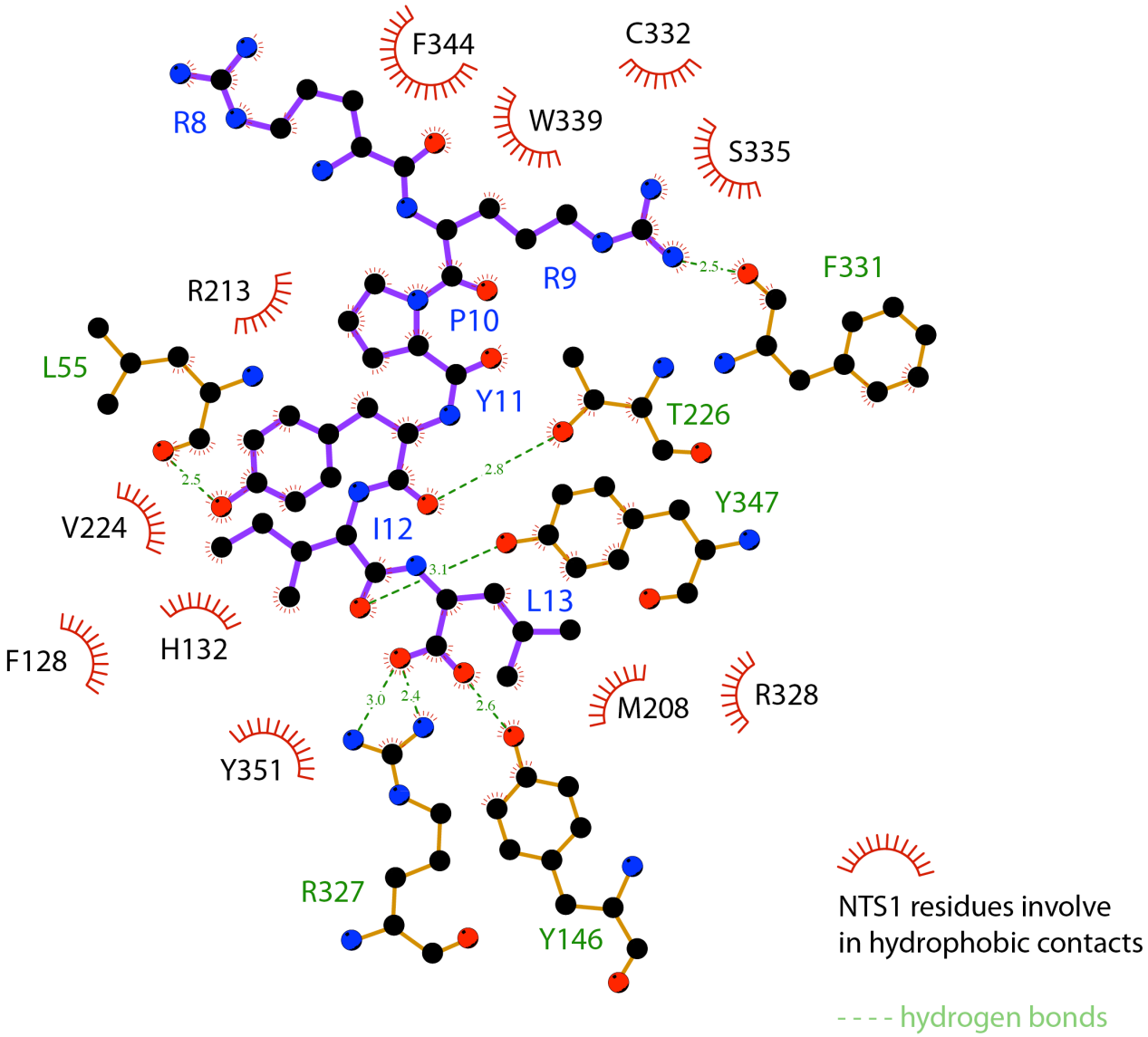

Fig. S10: Stereo view of the NTS1-GW5-T4L agonist binding pocket.

NT_{8-13} is shown as stick model. The receptor residues (grey labels) in contact with the peptide ligand (bold black labels) are depicted. Hydrogen bonds and salt bridges are indicated by dashed lines. The ECL2 with the β-hairpin is colored in pink.

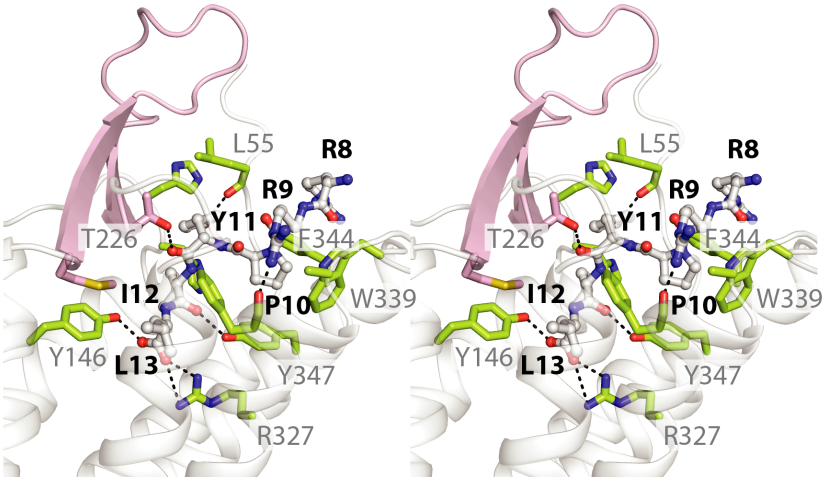

Fig. S11: Quality of the electron density for the agonist in the NTS1-GW5-T4L structure.

(Top) The F_o-F_c omit map is indicated in green (NT_{8-13} omitted, contoured at 2σ), stereo view. (Bottom) The final $2F_o$-F_c map is shown in grey (contoured at 1σ). The agonist model is shown as sticks and its amino acid side chains are labeled.

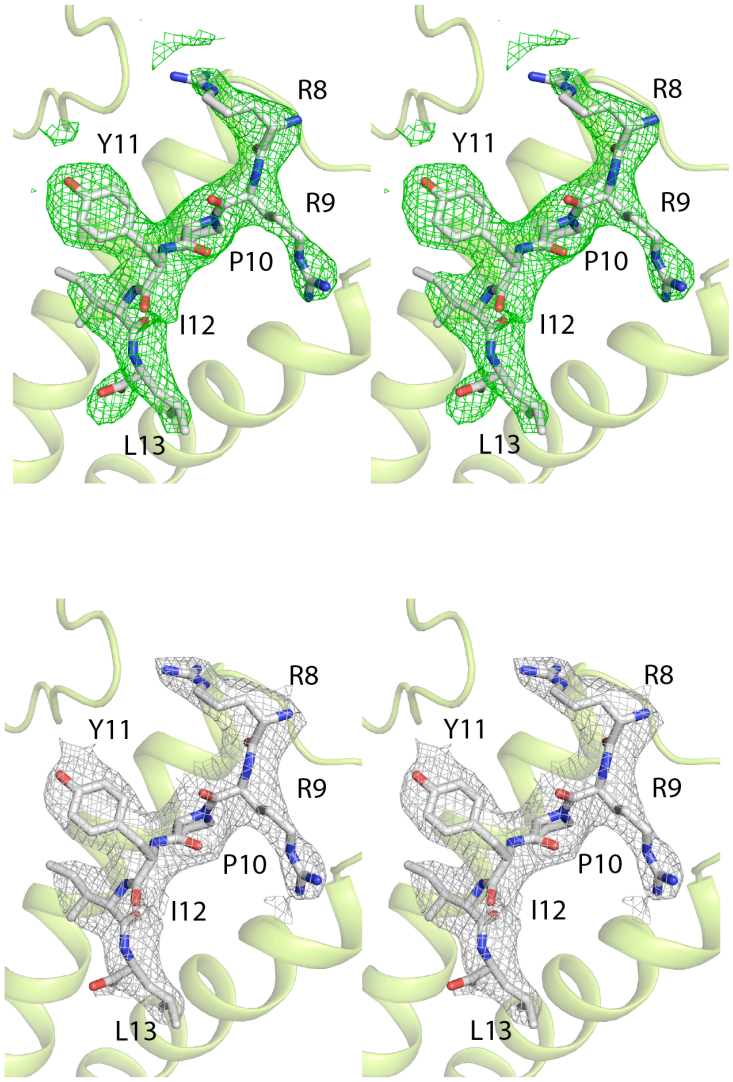

Fig. S12: Possible decarboxylation of the NT peptide caused by radiation damage.

Shown is an NT_{8-13} F_o-F_c omit map in green contoured at 2σ. The Cα atom of L13 is labeled. The putative salt-bridge like interaction of the cleaved entity with R327 in TM6 is indicated by dashed lines. The nature of the electron density adjacent to the side chain of R327 is unclear. It appears to be too large for a H_2O molecule and is inconsistent with CO_2. We have therefore modeled it as formate.

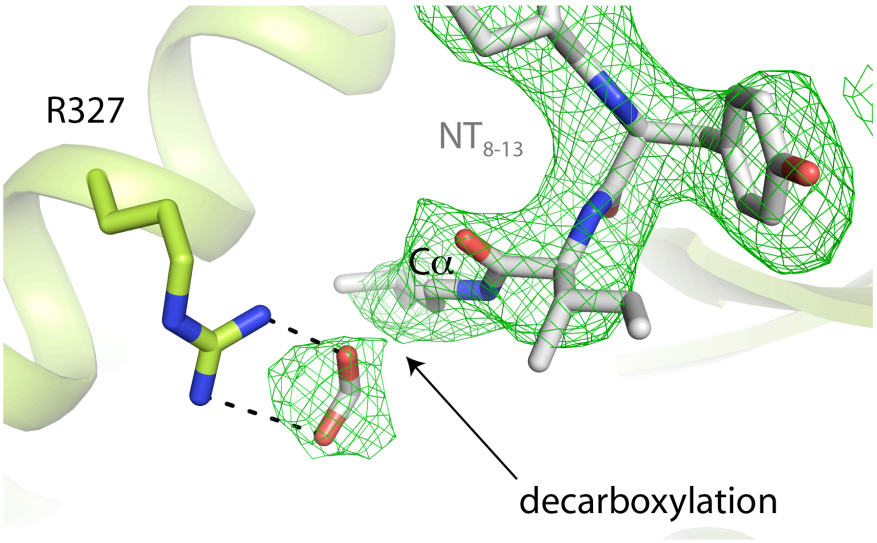

Fig. S13: The backbone conformation of NT_{8-13} is similar for the agonist bound to NTS1-GW5-T4L and wild-type NTS1.

Main chain atoms are shown for the peptide bound to NTS1-GW5-T4L (yellow, crystal structure) and to wild-type NTS1 (green, solid state NMR study[22]). The NMR data predicted a family of backbone structures and the backbone torsion angles of NT_{8-13} shown here fall within this ensemble.

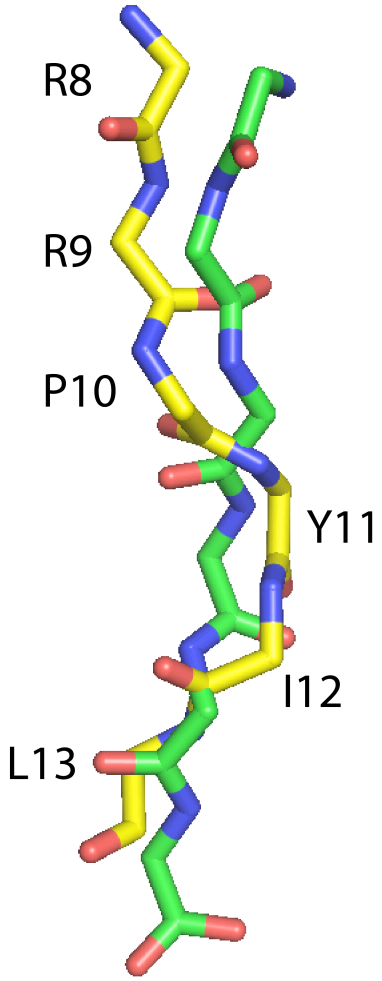

Fig. S14: Helical kink of TM2.

Extracellular view of the NTS1-GW5-T4L structure (green). The agonist NT_{8-13} is shown as stick model. The pronounced helical kink of TM2 at $A120^{2.57}$ allows the extracellular end of TM2 to bend towards the receptor center. Residue F128 that forms part of the peptide ligand binding pocket is labeled. The CXCR4 receptor[23] is shown for comparison in yellow. The positions of the extracellular ends of TM2 in the opioid receptors[24-27] are similar to that of the chemokine receptor (not shown).

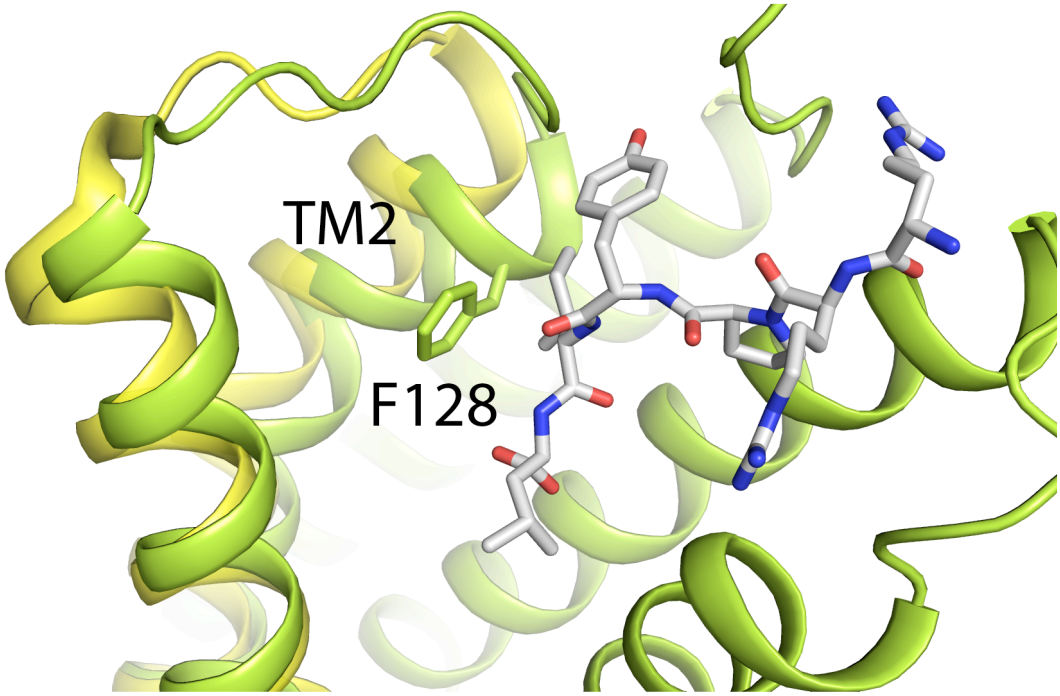

Supplemental references

1 Gully, D. *et al.* Biochemical and pharmacological profile of a potent and selective nonpeptide antagonist of the neurotensin receptor. *Proc. Natl. Acad. Sci. U.S.A.* **90**, 65-69 (1993).

2 Shibata, Y. *et al.* Thermostabilization of the neurotensin receptor NTS1. *J. Mol. Biol.* **390**, 262-277 (2009).

3 Liu, W. *et al.* Structural basis for allosteric regulation of GPCRs by sodium ions. *Science* **337**, 232-236 (2012).

4 Martin, S., Botto, J. M., Vincent, J. P. & Mazella, J. Pivotal role of an aspartate residue in sodium sensitivity and coupling to G proteins of neurotensin receptors. *Mol. Pharmacol.* **55**, 210-215 (1999).

5 Lebon, G., Bennett, K., Jazayeri, A. & Tate, C. G. Thermostabilisation of an agonist-bound conformation of the human adenosine A(2A) receptor. *J. Mol. Biol.* **409**, 298-310 (2011).

6 Barroso, S. *et al.* Identification of residues involved in neurotensin binding and modeling of the agonist binding site in neurotensin receptor 1. *J. Biol. Chem.* **275**, 328-336 (2000).

7 Botto, J. M. *et al.* Identification in the rat neurotensin receptor of amino-acid residues critical for the binding of neurotensin. *Mol. Brain Res.* **46**, 311-317 (1997).

8 Labbe-Jullie, C. *et al.* Mutagenesis and modeling of the neurotensin receptor NTR1. Identification of residues that are critical for binding SR 48692, a nonpeptide neurotensin antagonist. *J. Biol. Chem.* **273**, 16351-16357 (1998).

9 Richard, F., Barroso, S., Nicolas-Etheve, D., Kitabgi, P. & Labbe-Jullie, C. Impaired G protein coupling of the neurotensin receptor 1 by mutations in extracellular loop 3. *Eur. J. Pharmacol.* **433**, 63-71 (2001).

10 Henry, J. A., Horwell, D. C., Meecham, K. G. & Rees, D. C. A structure-affinity study of the amino acid side-chains in neurotensin: N and C terminal deletions and Ala-scan. *Bioorg. Med. Chem. Lett.* **3**, 949-952 (1993).

11 Labbe-Jullie, C. *et al.* [3H]SR 48692, the first nonpeptide neurotensin antagonist radioligand: characterization of binding properties and evidence for distinct agonist and antagonist binding domains on the rat neurotensin receptor. *Mol. Pharmacol.* **47**, 1050-1056 (1995).

12 Chen, V. B. *et al.* MolProbity: all-atom structure validation for macromolecular crystallography. *Acta Crystallogr. D Biol. Crystallogr.* **66**, 12-21 (2010).

13 Krissinel, E. & Henrick, K. Inference of macromolecular assemblies from crystalline state. *J. Mol. Biol.* **372**, 774-797 (2007).

14 Fredriksson, R., Lagerstrom, M. C., Lundin, L. G. & Schioth, H. B. The G-protein-coupled receptors in the human genome form five main families. Phylogenetic analysis, paralogon groups, and fingerprints. *Mol. Pharmacol.* **63**, 1256-1272 (2003).

15 Ballesteros, J. A. & Weinstein, H. Integrated methods for the construction of three-dimensional models and computational probing of structure-function relations in G protein-coupled receptors. *Methods Neurosci.* **25**, 366-428 (1995).

16 Kabsch, W. & Sander, C. Dictionary of protein secondary structure: pattern recognition of hydrogen-bonded and geometrical features. *Biopolymers* **22**, 2577-2637 (1983).

17 Rasmussen, S. G. *et al.* Crystal structure of the beta2 adrenergic receptor-Gs protein complex. *Nature* **477**, 549-555 (2011).

18 Choe, H. W. *et al.* Crystal structure of metarhodopsin II. *Nature* **471**, 651-655 (2011).

19 Vita, N. *et al.* Cloning and expression of a complementary DNA encoding a high affinity human neurotensin receptor. *FEBS Lett.* **317**, 139-142 (1993).

20 Tanaka, K., Masu, M. & Nakanishi, S. Structure and functional expression of the cloned rat neurotensin receptor. *Neuron* **4**, 847-854 (1990).
21 Wallace, A. C., Laskowski, R. A. & Thornton, J. M. LIGPLOT: A program to generate schematic diagrams of protein-ligand interactions. *Protein Eng.* **8**, 127-134 (1995).
22 Luca, S. *et al.* The conformation of neurotensin bound to its G protein-coupled receptor. *Proc. Natl. Acad. Sci. U.S.A.* **100**, 10706-10711 (2003).
23 Wu, B. *et al.* Structures of the CXCR4 chemokine GPCR with small-molecule and cyclic peptide antagonists. *Science* **330**, 1066-1071 (2010).
24 Granier, S. *et al.* Structure of the delta-opioid receptor bound to naltrindole. *Nature* **485**, 400-404 (2012).
25 Manglik, A. *et al.* Crystal structure of the mu-opioid receptor bound to a morphinan antagonist. *Nature* **485**, 321-326 (2012).
26 Thompson, A. A. *et al.* Structure of the nociceptin/orphanin FQ receptor in complex with a peptide mimetic. *Nature* **485**, 395-399 (2012).
27 Wu, H. *et al.* Structure of the human kappa-opioid receptor in complex with JDTic. *Nature* **485**, 327-332 (2012).